

Identifying a Transition Climate Zone in an Arid River Basin using Evaporative Stress Index

Yongqiang Liu¹, Lu Hao², Decheng Zhou², Cen Pan², Peilong Liu², Zhe Xiong³, Ge Sun⁴

¹Center for Forest Disturbance Science, USDA Forest Service, Athens, Georgia, USA

²Jiangsu Key Laboratory of Agricultural Meteorology, International Center for Meteorology, Ecology, and Environment, College of Applied Meteorology, Nanjing University of Information Science and Technology, Nanjing, China

³Institute of Atmospheric Physics, Chinese Academy of Sciences, Beijing, China

⁴Eastern Forest Environmental Threat Assessment Center, USDA Forest Service, Raleigh, North Carolina, USA

Correspondence to: Yongqiang Liu (yongqiang.liu@usda.gov), Lu Hao

Abstract. Aridity indices have been widely used in climate classification. However, there is not enough evidence for their ability in identifying the multiple climate types in areas with complex topography and landscape, especially in those areas with a transition climate. This study compares a traditional meteorological aridity index (*AI*), defined as the ratio of precipitation (*P*) to potential evapotranspiration (*PET*), with a hydrological aridity index, the Evaporative Stress Index (*ESI*) defined as the ratio of actual evapotranspiration (*AET*) to *PET*. in the Heihe River Basin (HRB) of the arid northwestern China. *PET* was estimated using the Penman-Monteith and Hamon methods. The aridity indices were calculated using the high resolution climate data simulated with a regional climate model for the period of 1980-2010. The climate classified by *AI* shows a climate type for the upper basin and a second type for the middle and lower basin, while three different climate types are found using *ESI*, each for one river basin, indicating that only *ESI* is able to identify a transition climate zone in the middle basin. The difference between the two indices is also seen in the inter-annual variability and extreme dry / wet events. The magnitude of variability in the middle basin is close to that in the lower basin for *AI*, but different for *ESI*. *AI* had larger magnitude of the relative inter-annual variability and greater decreasing rate from 1980-2010 than *ESI*, suggesting the role of local hydrological processes in moderating extreme climate events. Thus, the hydrological aridity index is better than the meteorological aridity index for climate classification in the arid Heihe River Basin.

36 **1 Introduction**

37

38 Aridity indices combine one or several variables (indicators) into a single numerical value to measure water
39 deficit over long periods (e.g., 30 years or longer) (Wilhite and Glantz, 1985, Zargar et al., 2011). Aridity
40 indices are useful tool for climate classification
41 (https://en.wikipedia.org/wiki/Climate_classification). In comparison with comprehensive tools such
42 as the Koppen climate classification (Peel et al., 2007), aridity indices do not need complex
43 information on the properties of ecosystems and therefore are used more easily and often at local and
44 regional scales.

45

46 Aridity indices can be categorized into different types including meteorological and hydrological indices, which
47 could be simply considered as a lack of water due to anomalous atmospheric and land-surface conditions,
48 respectively. Precipitation, temperature and humidity are atmospheric conditions often used to estimate
49 meteorological aridity indices. The earliest aridity index, developed more than a century ago, reflects the effects of
50 the thermal regime and the amount and distribution of precipitation in determining the native vegetation possible
51 in an area. By the middle of the 20th century, attentions turned to precipitation and potential evaporation (Huschke,
52 1959). A typical index of this type, the Budyko-type aridity index (AI) (Budyko, 1974), for example,
53 uses annual averages of precipitation and potential evapotranspiration (PET), which is mainly
54 determined by temperature.

55

56 Land-surface conditions such as streamflow, runoff, and actual evapotranspiration are often used to
57 estimate hydrological aridity indices (Maliva and Missimer, 2012). The Evaporative Stress Index
58 (ESI), for example, defines dryness degree based on the ratio of actual evapotranspiration (AET) to
59 PET over both short and long periods. A relatively low ESI indicates water limitation to plants and the
60 actual rate is way below the PET. In contrast, a relatively high ESI indicates freely available water
61 with the AET rate approaching or close to the PET. The ESI has been used to evaluate the irrigation
62 need for crop growth and land classification (Yao, 1974). The ESI was used recently to evaluate water
63 stress using remotely sensed hydrological and ecological properties (Anderson et al., 2016).

64

65 There are many similarities between aridity indices and drought indices, which measure water deficit
66 over short periods (such as months, seasons, and years). Drought indices also are categorized into

67 meteorological, hydrological, and other types. Percent of Normal (PN) and Standardized Precipitation
68 Index (SPI) (McKee et al., 1993) are simply based on precipitation and can be used to measure
69 anomalies of a period over various lengths. Palmer Drought Severity Index (PDSI) (Palmer, 1965)
70 and Keetch-Byram Index model (Keetch and Byram, 1968) are based on water supply and demand
71 estimated mainly using precipitation and temperature (Guttman, 1999). Both PDSI and KBDI
72 depend on precedent daily or monthly values, making them specifically useful for a persistent event
73 like drought. Among various hydrological drought indices, Streamflow Drought Index (SDI) (Nalbantis
74 and Tsakiris, 2009) and Surface Water Supply Index (SWSI) (Shafer and Dezma, 1982) use
75 streamflow as well as reservoir storage and precipitation to monitor abnormal surface water
76 (Narasimhan and Srinivasan, 2005). Standardize Runoff Index (SRI) (Shukla and Wood, 2008) is
77 standard normal deviate associated with runoff accumulated over a specific duration.

78
79 Large river basins at continental and sub-continental scales usually encompass multiple
80 climate types related to complex topography and landscape. Climate is more humid in the
81 upper basin near the river origins with high elevations and forest and / or permanent snow
82 cover than the lower basin with low elevations and less vegetated lands. Climate could be
83 extremely dry in parts of a watershed under a prevailing atmospheric high-pressure system.
84 The sub-continental Colorado River watershed, for example, is dominated by cold and humid
85 continental climate in the upper basin of the Rocky Mountains and cold semi-arid or warm
86 desert climate in the lower basin of the southern inter-mountains.

87
88 This feature of multiple climate types is also seen in some smaller basins. The Heihe River
89 Basin (HRB) in northwestern China, for example, has an area of 130, 000 km² with annual
90 precipitation varying dramatically from about 500 mm in the upper basin of the Qilian
91 Mountains with forest-meadow-ice covers in the south to less than 100 mm in the lower basin
92 of the Alxa High Plain with Gobi and sandy lands in the north. Climate types change from cold
93 and humid continental to arid desert, accordingly.

94
95 The relative high precipitation in the humid upper basin supports forests and meadows and
96 provides source water lower reach of the Heihe River. In contrast, water is a major limitation
97 factor in arid lower basin. In addition, more extreme weather conditions, especially droughts,

98 occur in arid lower basin. In the Colorado River basins, the reconstructed data show decadal
99 periods of persistently low flows during the past centuries (Woodhouse et al., 2010). The
100 drought severity in the new millennia has been the most extreme over a century (Cayan et al.,
101 2010). The reconstructed precipitation series in the HRB indicates that droughts were much
102 more frequent and lasted longer than floods in the past two centuries (Ren et al., 2010).
103 Droughts occurred more often in the dry lower basin than the humid upper basin (Li, 2012).
104

105 The watersheds with varied topography and landscape may have a transition climate zone
106 between the two zones. In the HRB, for example, the Koppen climate classification, one of the
107 most widely used climate classification techniques at large geographic scales and constructed
108 based on the properties of ecosystems, latitude, and average and seasonal precipitation and
109 temperature, shows polar tundra or boreal climate in the upper basin of the mountain regions
110 in the south, arid desert climate in the lower basin in the north, and a transition zone of steppe
111 climate in the middle. Identifying this transition zone and understanding its unique climate
112 features are of both scientific and management significance. The complex topography in upper
113 basin and harsh climate in lower basin make both regions unsuitable for human living. The
114 transition zone however is relatively flat in comparison with the mountain region and less arid
115 in comparison with the dryland region. It therefore provides a favorable condition for industrial
116 and agricultural development. Also, the environmental conditions in this region are more
117 dynamical and localized because of human induced rapid and fragmental landscape changes.
118

119 ESI is similar to AI but more related to surface hydrology. However, unlike AI, ESI applications for
120 climate classification have yet been conducted. In addition, many studies have compared ESI with
121 other drought indices in different climatic environments. For example, Otkin et al. (2013) compared
122 the ESI with drought classification used by the U.S. Drought Monitor (USDM) (Svoboda et al., 2002)
123 and found that the ESI anomalies led the USDM drought depiction by several weeks and large ESI
124 anomalies therefore were indicative of rapidly drying conditions. This finding was coincident with the
125 droughts occurred across the United States in recent years. Choi et al. (2013) compared the ESI with
126 the Palmer drought severity index (PDSI) in a watershed of the Savannah River branch in southeastern
127 United States during 2000-2008. They found that the ability of the ESI to capture shorter term
128 droughts was equal or superior to the PDSI when characterizing droughts for the watershed with a

129 relatively flat topography dominated by a single land cover type. However, the differences
130 between ESI and meteorological indices in capturing the spatial patterns under complex
131 topography and environments are not well characterized and understood.

132

133 This study is to compare the capacity of the hydrological aridity index, ESI and the meteorological
134 aridity index, AI, in climate classification, especially in identifying a possible transition
135 climate zone in the HRB. These two indices reflect the water (precipitation and
136 evapotranspiration) and heat (radiation) properties on the ground surface without the
137 needs to obtain the complex vegetation and soil hydrological properties. The surface
138 properties needed to calculate ESI and AI could be obtained from regional climate
139 modeling, which was an approach used in this study. The analysis of the climate zones was
140 made by comparing the spatial patterns and regional averages. Their temporal variations were also
141 analyzed to understand the differences in the seasonal and inter-annual variability and long-term
142 between ESI and AI.

143

144 **2 Methods**

145 **2.1 Study region**

146

147 The study region was the HRB and the adjacent areas (Fig. 1). The Heihe River originates from
148 the Qilian Mountains in the northern edge of the Tibet Plateau and flows northward to the
149 China-Russian border. The HRB spans between 98°~101°30'E and 38°~42°N. The upper HRB
150 is within the mountains elevated 2300~3200m mainly covered with forests and mountain
151 meadows. The middle HRB is along the Hexi Corridor elevated 1600~2300m mainly covered
152 with piedmont steppe grass, crops, and residence and commercial uses. The lower HRB is in
153 the Alxa High-Plain elevated below 1600m mainly covered with Gobi and desert sands.

154

155 Annual precipitation is over 400mm in the upper basin, with the maximum of 800mm at
156 extremely high elevations, about 100~250mm in the middle basin, and below 50mm in many
157 lower basin areas. The annual precipitation in the upper basin has high seasonal variability,
158 and nearly 70% of the total annual rainfall occurs from May to September (Gao et al., 2016).

159 The upper basin generates nearly 70% of the total river runoff, which supplies agricultural

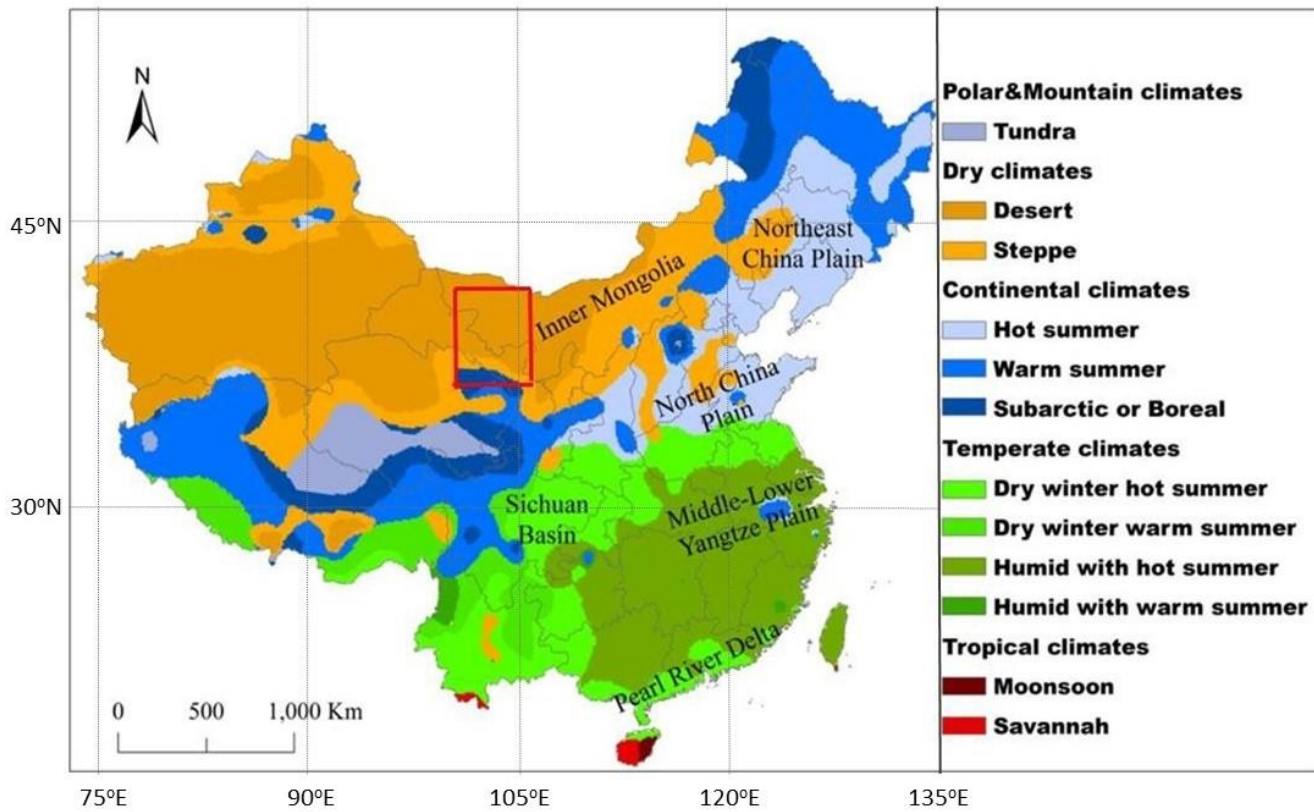
160 irrigation and benefits the social economy development in the middle and lower basin reaches
 161 (Yang et al., 2015; Chen et al., 2005). Annual mean temperature is about -4°C in the upper basin,
 162 7°C in the middle basin, and nearly 9°C in the lower basin.

163

164 2.2 Aridity indices

165

166 The meteorological aridity index is defined as $AI = P / PET$, where P and PET are daily
 167 precipitation and potential evapotranspiration, respectively. AI is a variant of the index
 168 originally defined by Budyko (1974), which is the ratio of annual PET to P . The average AI
 169 values were used to classify the arid, semi-arid, semi-humid (sub-humid), and humid climate
 170 with the ranges of $AI \leq 0.2$, $0.2 < AI \leq 0.5$, $0.5 < AI \leq 1.3$, and $AI > 1.3$, respectively (Ponce et al.,
 171 2000).



172

173 Figure 1. The study region of the Heihe River Basin (red box) in China and the Koppen climate
 174 classification (from Peel et al., 2007).

175

176 The hydrological aridity index is defined as $ESI = AET / PET$, where AET is daily actual

177 evapotranspiration. The ranges of average ESI values of $ESI \leq 0.1$, $0.1 < ESI \leq 0.3$, $0.3 < ESI$
 178 ≤ 0.6 , and $ESI > 0.6$ were used to classify the arid, semi-arid, semi-humid, and humid climate,
 179 respectively (Yang, 2007). This approach agrees with Anderson (2011), which showed that the
 180 ESI values varying gradually from 0 to 1 correspond to several USDM drought levels from
 181 exceptional to no drought for each month from April to September across the continental U.S.

182

183 Two methods were used to estimate *PET* (mm/d). One was the energy balance based FAO-

184 56 Penman-Monteith Equation (Allen et al. 1998):

185

$$186 \quad PET_p = \frac{0.408\Delta(NRAD - G) + 900\gamma u_2(e_s - e)/(T + 273)}{\Delta + \gamma(1 + 0.34u_2)} \quad (1)$$

187

188 where *NRAD* and *G* are net radiation and soil flux on the ground ($\text{MJm}^{-2}\text{d}^{-1}$); *T* is air temperature
 189 ($^{\circ}\text{C}$); e_s and e are saturation and actual water vapor pressure (kPa); u_2 is wind speed at 2m above
 190 the ground (ms^{-1}); Δ is the rate of change of e_s with respect to T ($\text{kPa}/^{\circ}\text{C}$); γ is the psychrometric
 191 constant ($\text{kPa}/^{\circ}\text{C}$). The other method is the temperature based on Hamon formula (Hamon,
 192 1963):

193

$$194 \quad PET_h = (k \times 0.165 \times 216.7 \times N \times e_s) / (T + 273.3) \quad (2)$$

195

196 where k is proportionality coefficient = 1; N is daytime length. e_s is in 100 Pa here.

197

198 Monthly *PET*, precipitation and actual evapotranspiration, obtained based on daily values, were
 199 used to calculate the aridity indices. It was assumed that daily $PET=0$ if daily $T < 0^{\circ}\text{C}$. Their
 200 monthly *PET* was not used if $PET=0$ for more than 10 days in a month. In this case, no aridity
 201 indices were calculated for the month. It was also assumed that daily ground energy was in
 202 balance, so $NRAD - G = H + L \times AET$, where H and L are sensible heat flux and potential heat constant.

203

204 T-test was conducted to obtain statistical significance of the differences in the aridity index values
 205 between two Heihe River reaches. The data used in calculation and evaluation of the aridity indices
 206 are listed in Table 1.

207

208 Table 1. The data used in calculation and evaluation of the aridity indices. H, AET, P, T, and
 209 e (RH) are sensible heat flux, actual evapotranspiration, precipitation, temperature, wind speed,
 210 and water vapor pressure (relative humidity). HRB stands for Heihe River Basin.
 211

Source	Parameter	Time Period	Space	Reference
Simulation	H, AET, P,T, u, e	1980-2010, daily	HRB, 3 km resolution	Xiong and Yan (2013)
Observation	P,T,RH	1980-2010, daily	3 sites in HRB	China National Met Sci Infrastructure (data.cma.cn)

212

213 **2.3 Regional climate modeling**

214

215 The climatic and hydrological data used to calculate the aridity indices were created from a
 216 regional climate modeling using the Regional Integrated Environmental Model System
 217 (RIEMS 2.0) (Xiong and Yan, 2013). The simulation was conducted over the period of 1980-
 218 2010. The horizontal spatial resolution was 3km. A unique feature with this simulation was
 219 that the model's parameters, including soil hydrological properties, were recalibrated based on
 220 observations and remote sensing data over the HRB that greatly improved the model's
 221 performance. The model evaluation indicated that the model was able to reproduce the spatial
 222 pattern and seasonal cycle of precipitation and surface *T*. The correlation coefficients between
 223 the simulated and observed pentad *P* were 0.81, 0.51, and 0.7 in the upper, middle, and lower
 224 HRB regions, respectively ($p < 0.01$).

225

226 The historical *T* and *P* observations during the simulation period at Yeilangou of the upper
 227 basin (38.25°N, 99.35°E, 3300 m above the sea level), Zhangye of the middle basin (38.11°N,
 228 100.15°E, 1484m), and Dingqing of the lower basin (40.3°N, 99.52°E, 1177m) were used to
 229 compare with the simulations. We also calculated SPI based on observed precipitation using a built-in
 230 function of the NCAR NCL (<https://www.ncl.ucar.edu/>). The results with measured precipitation
 231 were used to evaluate the model performance in simulating drought conditions.

232 **3 Results**

233

234 **3.1 Simulated climate and hydrology**

235

236 The spatial pattern of the simulated annual *T* averaged over the simulation period is featured

237 by the large changes between basin reaches, increasing from about -15°C in the tall mountains
238 of the upper basin to over 10°C in the deserts of the lower basin (Fig. 2). The simulated average
239 annual P shows an opposite gradient, decreasing from about 2.5 mm/d in the mountains to less
240 than 0.25 mm/d in the deserts (Fig. 2). The simulated $NRAD$ decreases from west to east in the mountains,
241 corresponding to an increasing trend in precipitation. $NRAD$ is small in the northeastern section of the
242 domain, probably due to large outgoing long-wave radiation related to clear and relative hot weather. The
243 simulated average annual AET has a similar pattern to precipitation (Fig. 2). The spatial variability is
244 much larger within the upper basin than the lower basin.

245
246 An interesting feature is that both T and P in the middle basin are very close to their
247 corresponding values in the lower basin but much different from those in the upper basin; the
248 AET difference between the middle and upper basin reaches however is much small.

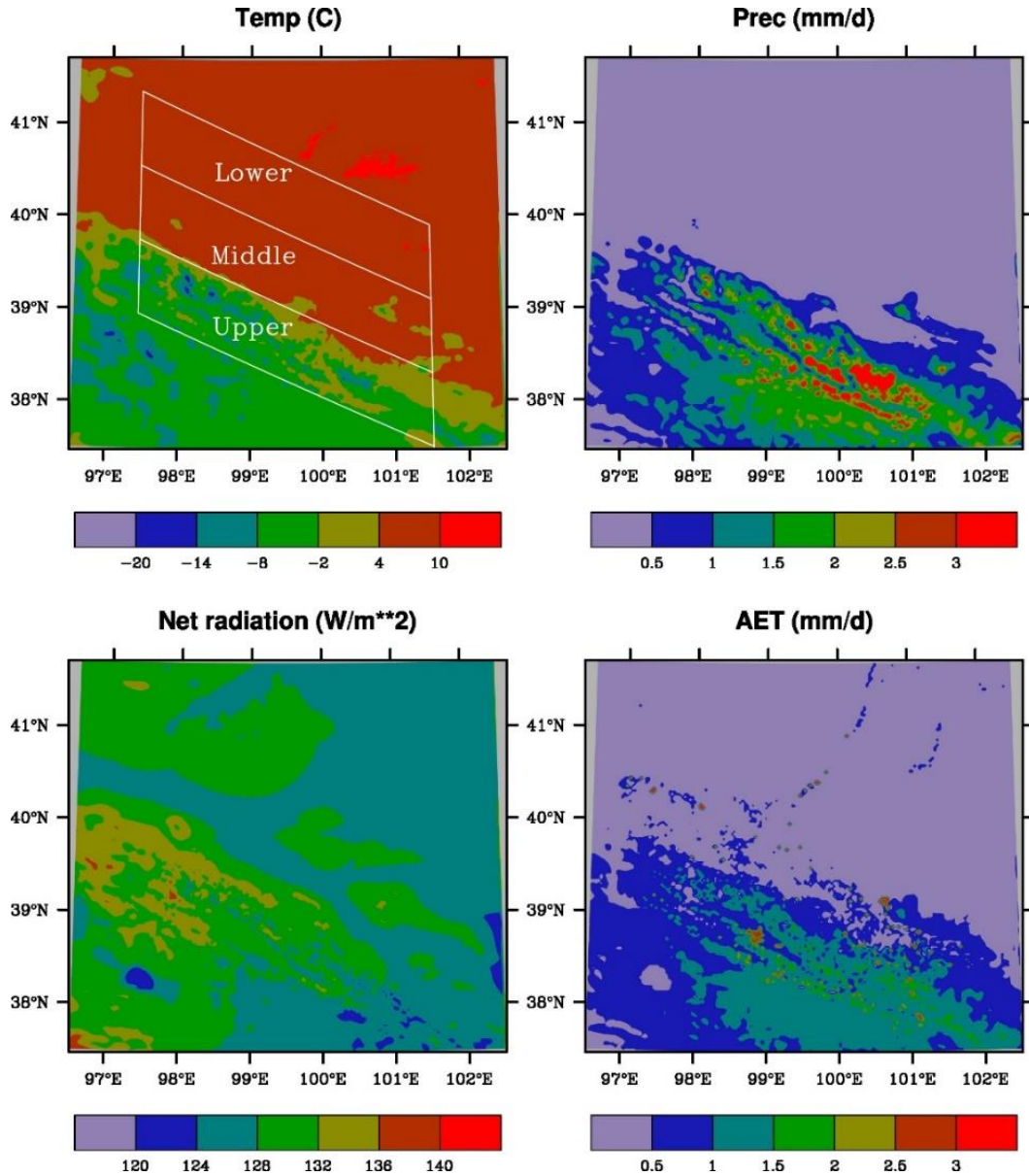


Figure 2. Spatial distributions of simulated air temperature (T , $^{\circ}\text{C}$), precipitation (P , mm/d), net radiation ($NRAD$, W/m^2) and actual evapotranspiration (AET , mm/d) averaged over 1980-2010. The Heihe River basins are shown in the left panel.

As expected, the regional AET values averaged over the simulation period are higher in summer than in winter (Fig. 3). In the upper basin, for example, T increases from about -15°C in winter to 10°C in summer, P increased from about 0.25 to 4 mm/d , and AET from about 0.25 to 2.5 mm/d . Again, T and P are close between the middle and lower basin reaches all seasons, and AET is close between the middle and upper basin reaches during winter and spring. While AET is

close between the middle and lower basin reaches during summer and fall, the differences between the middle and upper basin reaches are much smaller than the differences in T or P . Net radiation has s seasonal cycle similar to that of temperature. The changing trends among the three basin reaches are the same between T and $NRAD$ in Spring and Summer but opposite in Winter and Fall.

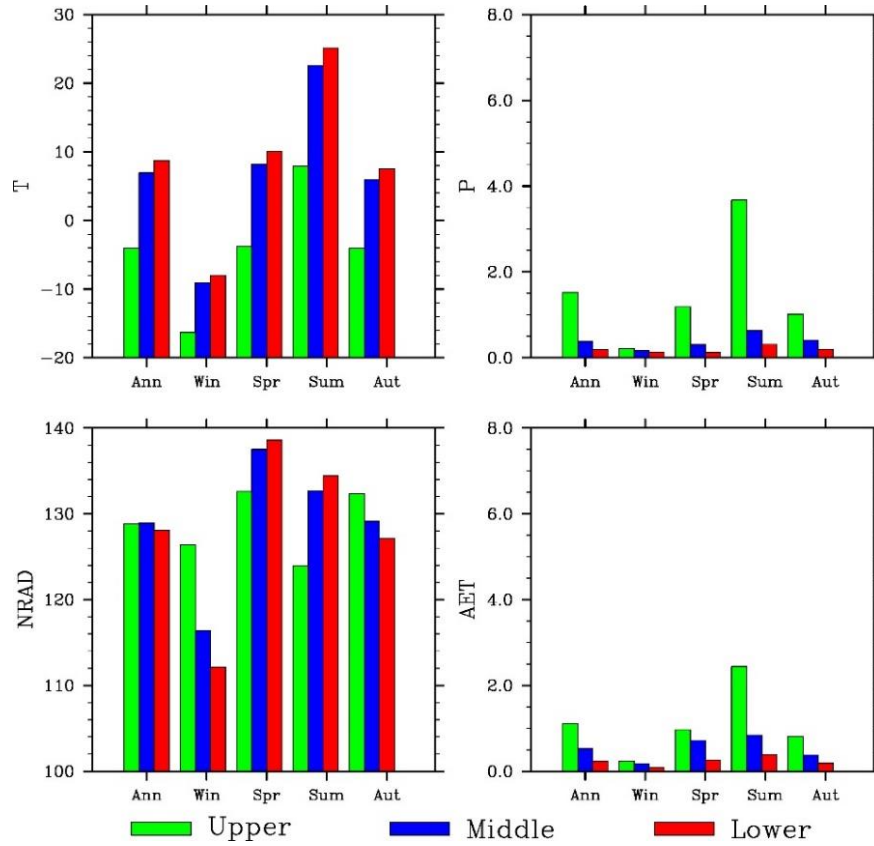


Figure 3. Seasonal variations of simulated air temperature (T , °C), precipitation (P , mm/d), net radiation ($NRAD$, W/m²) and actual evapotranspiration (AET , mm/d) in three basin reaches averaged over 1980-2010.

268 The inter-annual variability of regional T and P is similar between the middle and lower
269 basin reaches (Fig. 4). A few dry years (e.g., 1990, 2001, and 2008) and wet years (e.g., 1981,
270 1989, 2002, and 2007) can be found. The amplitude of variability is larger for P than T ,
271 especially in the upper basin. $NRAD$ values have large inter-annual variability with little difference
272 among the regions. The variability of AET is also similar between the lower and
273 middle basin reaches, but it differs from that in the upper basin during some periods (e.g.,
274 around 1985). The differences in AET between the middle and upper basins are much smaller
275 in the magnitude than those for the meteorological properties.

276

277 The above features of close values and similar inter-annual variability in the simulated T
278 and P between the middle and lower basin reaches are also seen in the observations (Fig. 4).
279 The simulated T in all basin regions and P in the middle and lower basin reaches are close to
280 the observed ones. However, the simulated P is about 0.4 mm/d higher (about 1.6 mm/d for
281 simulation vs. 1.2 mm/d for observation). The weather site in the upper basin is located in
282 relatively flat and low valley, while the simulation grids have many points at high elevations
283 where P is larger than at the valley locations.

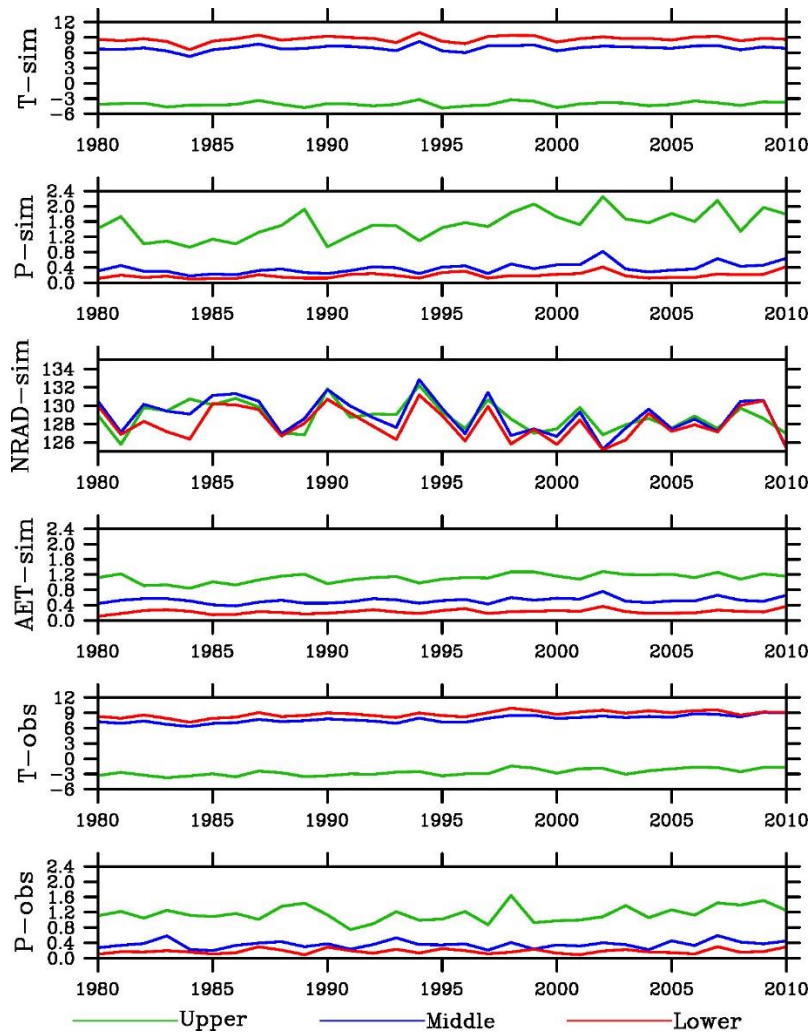


Figure 4. Inter-annual variations of simulated air temperature (T , °C), precipitation (P , mm/d), net radiation (NRAD, W/m^2) and actual evapotranspiration (AET , mm/d), and observed air temperature (T , °C) and precipitation (P , mm/d) in three basin reaches over 1980-2010.

The SPI for 12-month timescale also shows generally similar inter-annual variations over the analysis period between the simulated and observed precipitation in the three basins (Fig. 5). In the upper basin, for example, the observed wet spells occurred around 30, 50, 120, 230, 290, 340, and 360 months, while the dry spells occurred around 20, 30, 70, 100, 180, 200, 260, and 300 months. The simulation reproduces most of the wet and dry spells. However, the simulation is too wet during about 40-80 months and largely misses the dry events during 240-260 months.

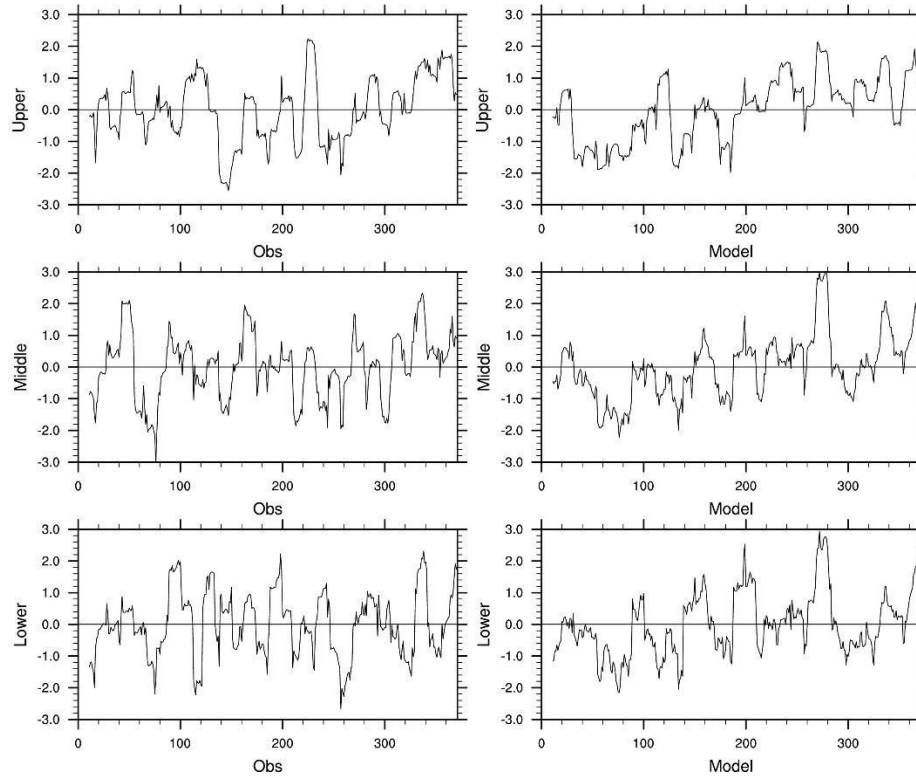


Figure 5. The Standardized Precipitation Index (SPI) for 12-month timescale over the analysis period. The left and right are observation and simulation. From top to bottom are the upper, middle, and lower basins, respectively. The horizontal number is month from the beginning of the analysis period.

The simulated P increases around 50% over the simulation period, statistically significant at $p < 0.01$ in all basin reaches (Table 2). The simulated AET also increases, but at a smaller degree of around 20% and $p < 0.01$ only in the upper basin. The simulated T shows increasing trends, but insignificant in all reaches. The simulated P trends are close to the observed ones in the middle and lower basin reaches, but opposite to that in the upper basin. The simulated T underestimates the observed warming, which was about 2°C at $p < 0.01$.

335 Table 2. Mann-Kendall trends from 1980 to 2010 of simulated temperature (T), precipitation
 336 (P), and actual evapotranspiration (AET) and observed temperature (T_{obs}), precipitation (P_{obs}).
 337 The bold and italic numbers are significant at $p<0.01$ and $p<0.05$, respectively.
 338

Variable	Upper	Middle	Lower
$T(^{\circ}C)$	0.4	0.4	0.4
P (%)	53.0	63.7	47.9
AET (%)	21.4	16.6	27.1
$T_{obs} (^{\circ}C)$	1.9	2.0	0.7
P_{obs} (%)	-10.7	74.6	62.5

339

340 3.2 Spatial patterns of aridity indices

341

342 PET calculated using the Penman-Monteith method is mostly 1.7-2.25 mm/d in the upper basin
 343 (Fig. 6). It increases to above 3 mm/d in the middle and lower basins. There is little difference
 344 between the two regions. The meteorological aridity index, AI , shows a similar pattern but
 345 opposite gradient (Fig. 6). It mostly has a humid climate in the upper basin, but becomes mainly arid
 346 climate in two other basin regions. The hydrological aridity index, ESI , has the same gradient as AI ,
 347 but with different spatial pattern (Fig. 6). It also mostly has a humid climate in the upper basin
 348 and arid climate in the lower basin. However, it is largely semi-arid climate in the middle basin. P
 349 and AET are the highest in the upper basin and the lowest in the lower basin, while T and PET have an
 350 opposite seasonal cycle. This explains why AI and ESI are larger in the upper basin than the middle or
 351 lower basin.

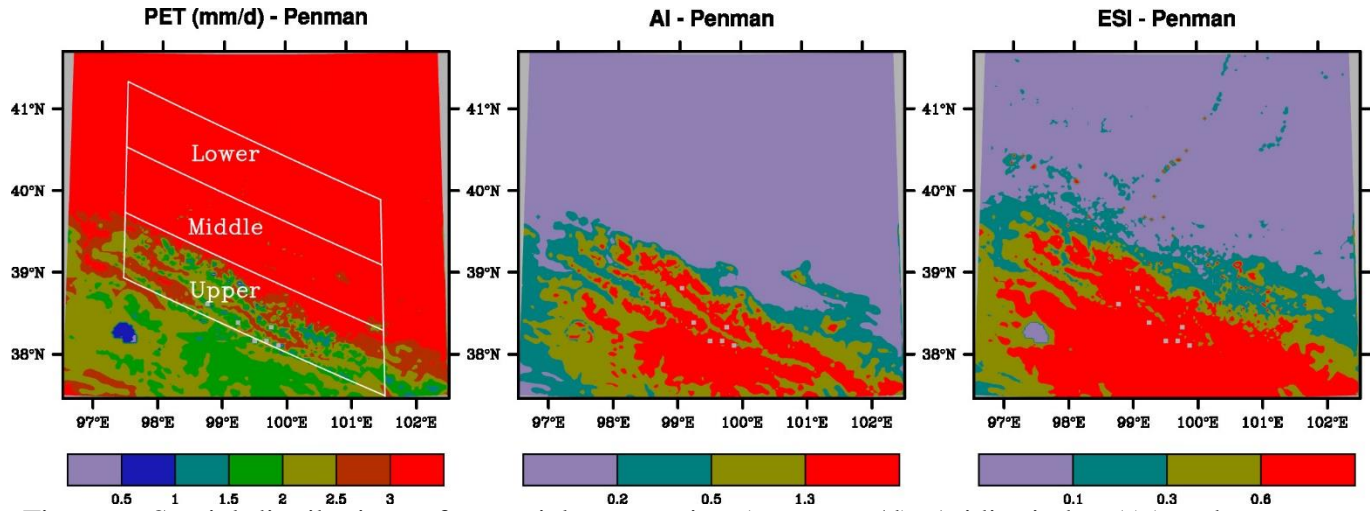


Figure 6. Spatial distributions of potential evaporation (PET , mm/d), Aridity index (AI) and Evaporative Stress Index (ESI) with PET estimated using the Penman-Monteith method. Averaged over 1980-2010. The Heihe River basins are shown in the left panel. The color bars from left to right for AI and ESI are arid, semi-arid, semi-humid and humid climate.

PET calculated using the Hamon method has the same pattern as the one using the Penman-Monteith method, but with smaller magnitude (Fig. 7). PET is mostly about 1 mm/d in the upper basin and increases to about 1.5-1.75 mm/d in the middle basin, and further to 1.75-2.25 mm/d in the lower basin.

The different spatial patterns between AI and ESI seen above are also found for the Homan method. AI is mostly above 0.6 in the upper basin (Fig. 7). It is below 0.2 in the middle and lower basins without apparent differences between the two regions. In contrast, while ESI remains large values of mostly above 0.9 in the upper basin and low values of below 0.2 in the lower basin, the values in many areas of the middle basin are 0.4-0.9, much different from those in the lower basin (Fig. 7).

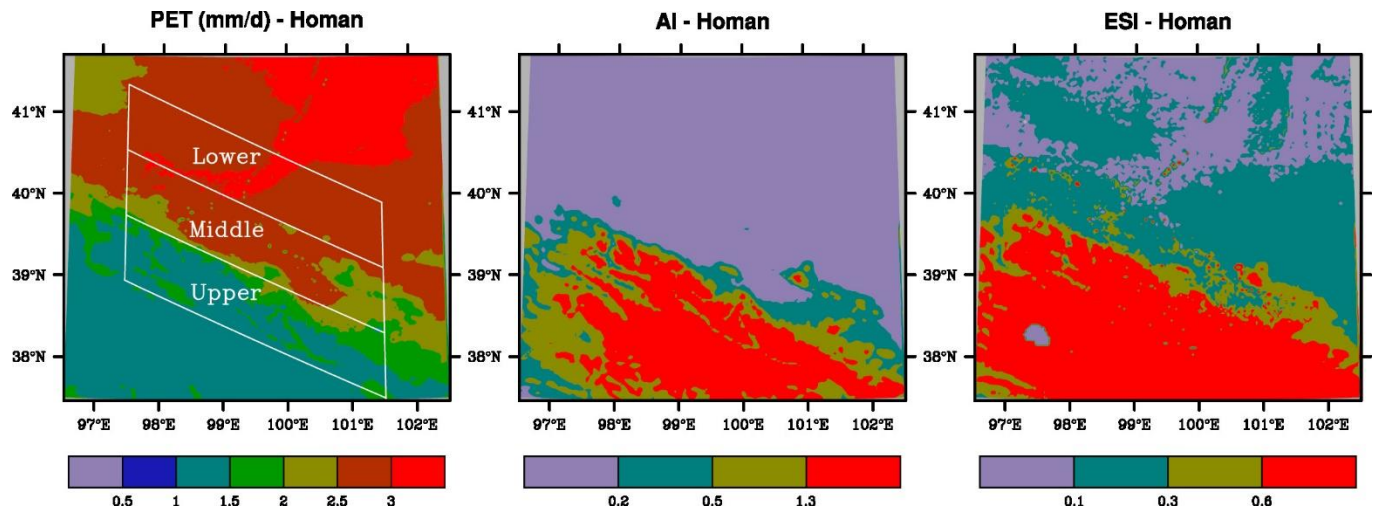


Figure 7. Spatial distributions of potential evaporation (PET , mm/d), Aridity index (AI) and Evaporative Stress Index (ESI) with PET estimated using the Hamon method. Averaged over 1980-2010. The Heihe River basins are shown in the left panel. The color bars from left to right for AI and ESI are arid, semi-arid, semi-humid and humid climate.

3.3 Climate classification

The annual PET averages over 1980-2010 calculated using the Penman method are 2.12, 3.91, and 4.76 (Table 3 and Fig. 8). The corresponding AI values are about 0.9, 0.12, and 0.04, falling into semi-humid, arid, and arid climate. The corresponding ESI values are 0.63, 0.22, and 0.07, falling into humid, semi-arid, and arid climate. The annual PET averaged over 1980-2010 calculated using the Homan method are 1.25, 2.33, and 2.65 mm/d for the upper, middle, and lower basin reaches. The corresponding AI values are about 1.3, 0.18, and 0.07, falling into humid, arid, and arid climate. The corresponding ESI values are 0.78, 0.31, and 0.13, falling into humid, semi-humid, and semi-arid climate. The averages of PET or each of the aridity index are statistically significant ($p < 0.01$) between any two regions of the Heihe River Basin.

Thus, the climate across the HRB classified using AI has two types of semi-humid (the Penman method for PET) or humid (the Homan method) in the upper basin, and arid in both middle and lower basin reaches. In contrast, the climate classified using ESI has three types of humid in the upper basin, semi-arid (the Penman method) or semi-humid (the Homan method) in the middle basin, and arid (the Penman method) or semi-arid (the Homan method) in the lower basin. This indicates that only the hydrological aridity index is able to identify the transition climate zone in the middle basin.

396 The difference between *AI* and *ESI* in classifying climate is related to the similar feature
397 with the meteorological variables. Annual *P* is 555 mm in the upper basin, which is
substantially different from 69-139 mm in the middle and lower basins. The mean *T* is -4.0°C
398 in the upper basin, which is well below 6.9-8.7°C in the middle and lower basin reaches. The
399 corresponding *PET* values fall into two groups, 299 mm in the upper basin and 672-767 mm
400 in the middle and lower basin reaches. This explains why the *AI* falls into two groups. In
401 contrast, *AET* is 226, 161, and 80 mm, substantially different not only between the middle and
402 upper reaches but also between the middle and lower reaches. This explains why the *ESI* falls
403 into three groups.

404
405 Table 3. Regional average (AVE), standard deviation (SD), and coefficient of variation (CV)
406 for potential evapotranspiration (*PET*, mm/d), aridity index (*AI*), and evaporative stress index
407 (*ESI*). A, SA, SH, and H represent arid, semi-arid, semi-humid, and humid climate, respectively.
408
409

PET	Basin	PET AVE	AI			ESI			SD	CV
			SD	CV	AVE	SD	CV	AVE		
Penman-Monteith	Upper	2.12	0.12	0.06	0.90 (SH)	0.32	0.35	0.62 (H)	0.07	0.11
	Middle	3.91	0.21	0.05	0.12 (A)	0.06	0.50	0.22 (SA)	0.06	0.26
	Lower	4.76	0.29	0.06	0.04 (A)	0.03	0.64	0.07 (A)	0.03	0.41
Hamon	Upper	1.25	0.04	0.03	1.30 (H)	0.37	0.29	0.78 (H)	0.05	0.07
	Middle	2.33	0.11	0.05	0.18 (A)	0.08	0.43	0.31 (SH)	0.06	0.19
	Lower	2.65	0.16	0.06	0.07 (A)	0.04	0.56	0.13 (SA)	0.04	0.31

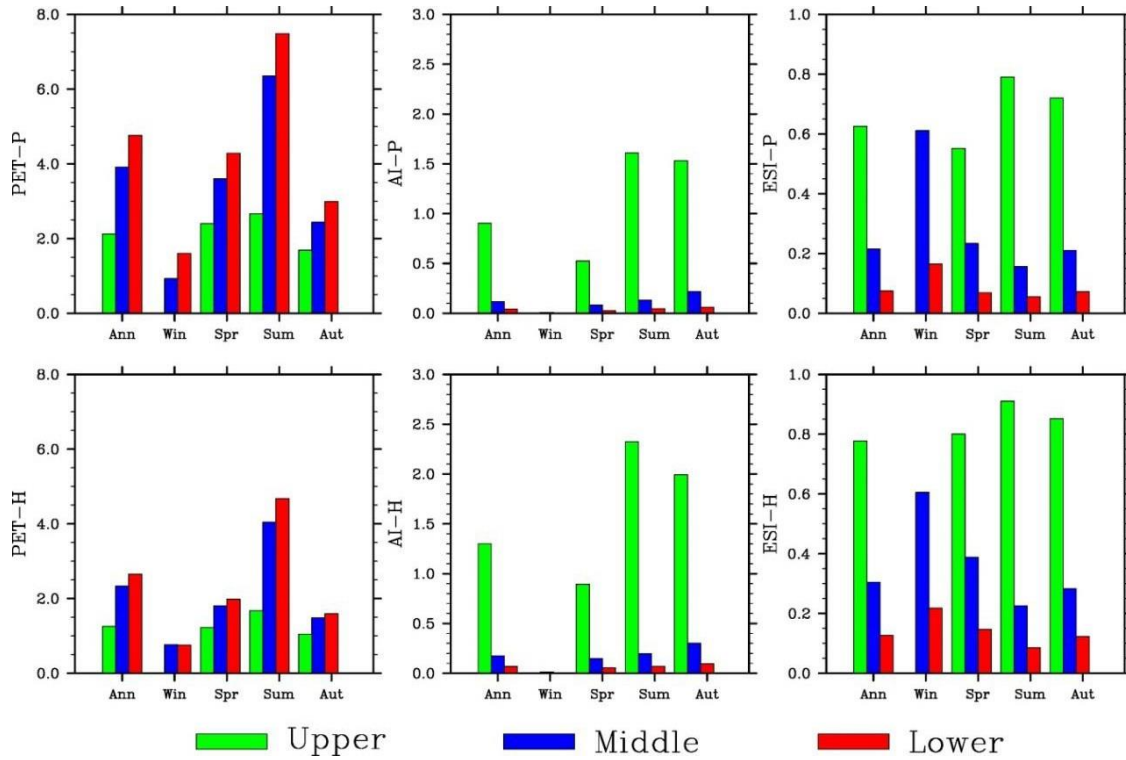


Figure 8. Seasonal variations of simulated potential evapotranspiration (PET , mm/d), Aridity Index (AI), and Evaporative Stress Index (ESI) (from left to right). The top and bottom panels are for the Penman-Monteith and Hamon method, respectively.

3.4 Temporal variations of aridity indices

3.4.1 Seasonal cycle

For the Penman-Monteith method, PET is the highest in summer and smallest in winter (Fig. 8). Note that winter PET in the upper basin is not shown because T is below zero on too many days. The amplitude in the middle basin is close to that in the lower basin, but much larger than that in the upper basin. Different from the upper basin where AI and ESI are also the largest in summer, AI is the largest in fall, while ESI is the largest in winter in the middle basin (as well as lower basin). The seasonal variations of PET , AI and ESI estimated using the Homan method are similar to those using the Penman method.

The seasonal AI and ESI cycles are related to those of the meteorological and hydrological conditions. T , P and AET (Fig. 3), and PET (Fig. 8) all increase from winter to summer. In the upper basin, the increases in P and AET from spring / fall to summer are larger than the

corresponding increases in *PET*, leading to larger *AI* and *ESI* values in summer. In the middle as well as lower basin, however, *PET* increases substantially from spring / fall, leading to smaller *AI* and *ESI* in summer than in spring / fall.

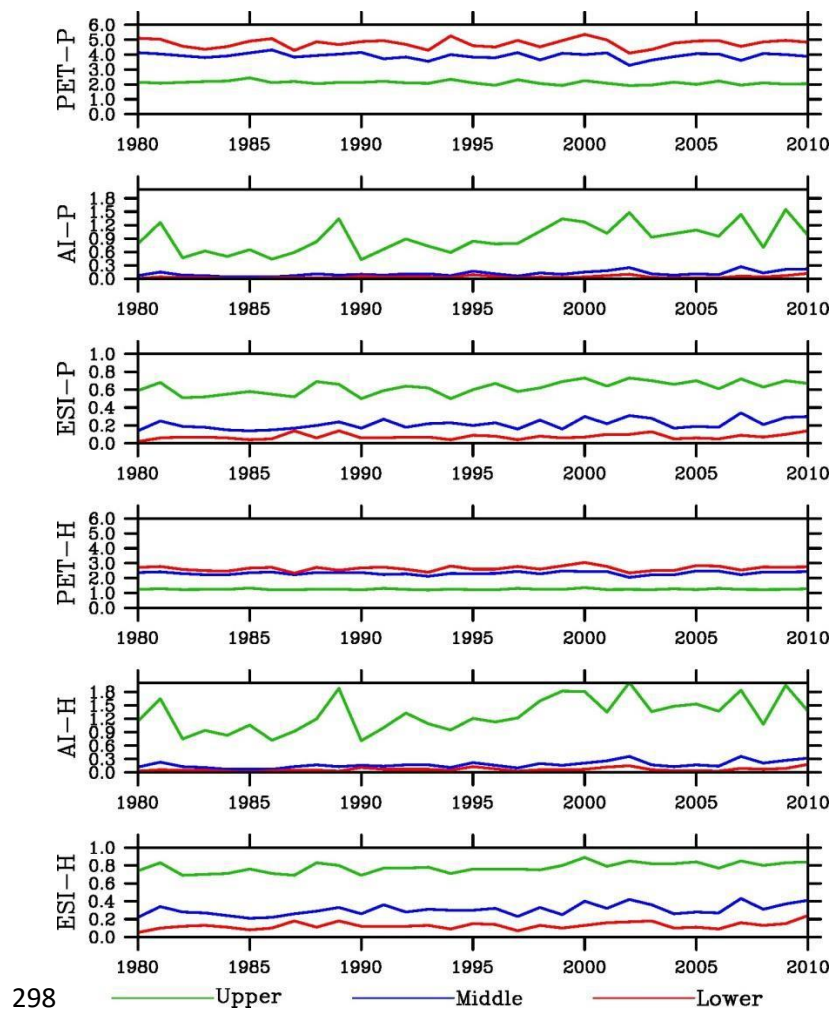
455

3.4.2 Inter-annual variability

457

PET in the middle basin calculated using the Penman-Monteith method shows similar inter-annual variability over the period of 1980-2010 to that in the lower basin, but much different from that in the upper basin (Fig. 9). The standard deviation (SD) increases from the upper (0.12) to middle (0.21) and to lower basin (0.29) (Table 2). The coefficient of variation (CV) (the ratio of the standard deviation to the average), a statistical property often used to measure relative variability intensity, however, is comparative among the reaches.

464



465

298

Figure 9. Inter-annual variations of potential evapotranspiration (*PET*, mm/d), Aridity Index (*AI*), and Evaporative Stress Index (*ESI*). P and H indicates the Penman-Monteith and Hamon method, respectively.

The SD values of both *AI* and *ESI* decrease from the upper to middle and to lower basin. However, SD of *AI* (*ESI*) in the middle basin is much closer to that in the lower (upper) basin. The CV values have opposite gradient to SD, increasing from the upper to middle and to lower basin. In addition, CV differs mainly not between the basin reaches but between aridity indices: *AI* is larger than *ESI*.

3.4.3 Long-term trends

PET shows little trends over the simulation period (Table 4). In contrast, aridity indices increased dramatically, by 60% or more for *AI* and 15-50% for *ESI*. The trends are significant at $p < 0.01$ in the upper and middle basin reaches and $p < 0.05$ in the lower basin. The results indicate a less dryness condition in the HRB, which is the more remarkable in the middle than upper basin and in the meteorological than hydrological aridity index. Increase in precipitation is a major contributor.

Table 4. Mann-Kendall trends from 1980 to 2010 of potential evapotranspiration (*PET*), Aridity Index (*AI*), and Evaporative Stress Index (*ESI*) (in%). *P* (*H*) indicates the Penman-Monteith (Hamon) method. The bold and italic numbers are significant at $p < 0.01$ and $p < 0.05$.

Index	Upper	Middle	Lower
PET-P	-7.3	-2.7	0.3
AI-P	72.5	98.6	<i>80.9</i>
ESI-P	24.8	51.4	<i>47.8</i>
PET-H	0.0	2.7	3.6
AI-H	62.6	84.3	<i>66.3</i>
ESI-H	16.2	40.8	<i>40.5</i>

3.5 Extreme events

The aridity indices for 4 simulated dry years (1982, 1990, 2001, and 2008) and 4 wet years (1981, 1989, 2002, and 2007) (Figs.10-11) and the averages over the dry or wet years (Fig. 12) were analyzed. The annual *AI* values using the Penman-Monteith method are 0.4-0.5 for the

494 first two dry years and 0.7-1.0 for the last two years in the upper valley (Fig. 12). The average
495 over the 4 years is about 0.65. In comparison, the average is about 0.9 over 1980-2010 and 1.4
496 over the 4 wet years. The values are very small in spring (except in 1982) and occasionally in
497 fall (1990). The annual *AI* values in the middle and lower basin reaches are below 0.2 for
498 individual dry years and average. The small values are found for individual seasons except
499 falls of the last two years in the middle basin. In comparison, the annual values are 0.4 or above
500 in 3 falls of the 4 wet years.

501
502 The annual *ESI* values using the Penman-Monteith method are 0.5 or larger in the upper
503 valley. The average over the 4 years are nearly 0.6. In comparison, the average is about 0.62
504 over 1980-2010 and 0.7 over the 4 wet years. The values are comparable from spring to fall,
505 though relatively smaller in spring. This is different from *AI*. The annual *ESI* values are about
506 0.2 in the middle and below 0.1 in the lower basin for individual dry years and average. Thus,
507 the values are apparently different between the middle and lower basin reaches. This is another
508 difference from *AI*. The lowest values mostly occur in summer in both basin reaches. In
509 comparison, the annual values are 0.25-0.35 in the middle basin and 0.1 or larger in 3 of the 4
510 wet years in the lower basin.

511
512 Same results can be found for the Hamon method, that is, substantially smaller *AI* than
513 normal, especially in spring but no much *ESI* changes from normal and between seasons in the
514 upper basin, and no much *AI* change from normal and wet events (small in all cases) in the
515 middle and lower basin reaches but much smaller *ESI* than wet events and different between
516 the two basin reaches, though slightly larger *AI* and *ESI* values. The results suggest that *ESI* is
517 better representative of extreme dry conditions in the middle basin, but less sensitive to aridity
518 in the upper basin.

519

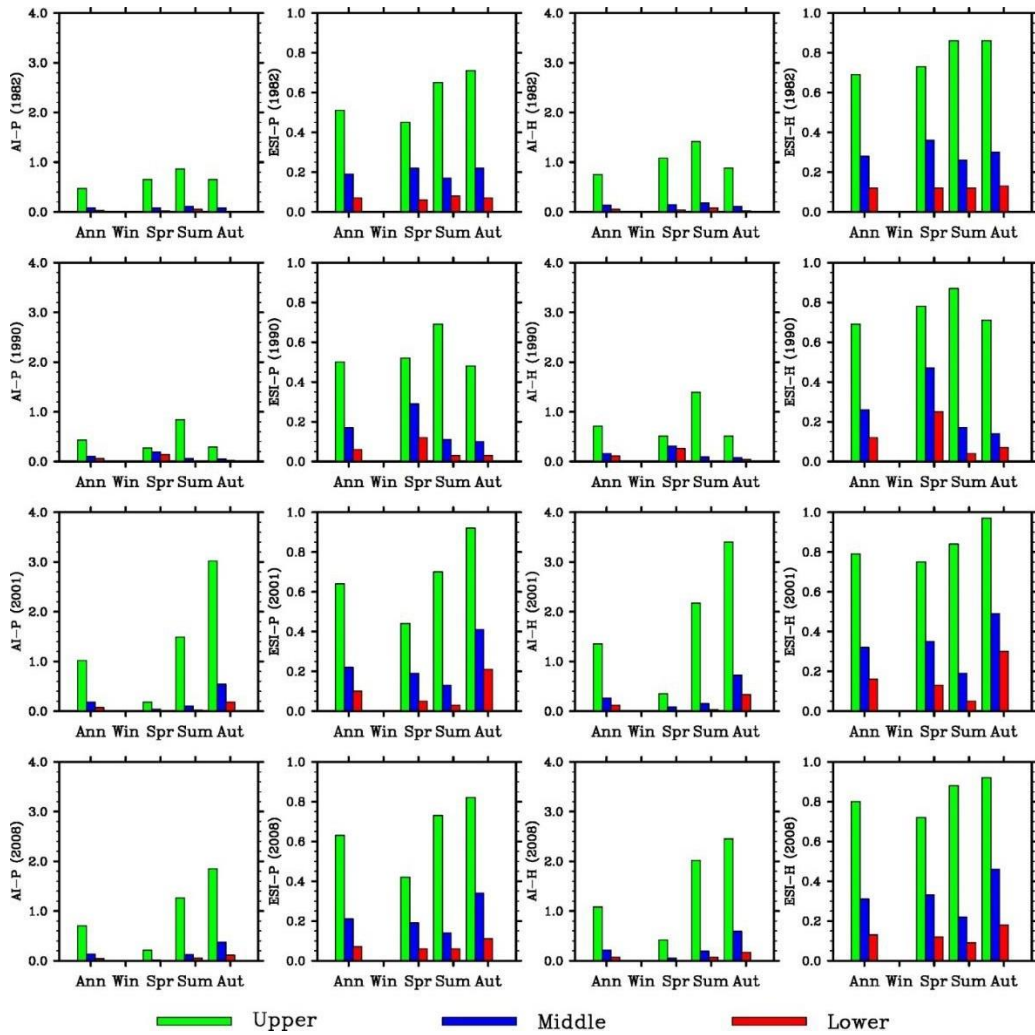


Figure 10. Seasonal variations of simulated Aridity Index (*AI*), and Evaporative Stress Index (*ESI*) using the Penman-Monteith and Hamon methods (left to right) for the dry years of 1982,1990, 2001, and 2008 (from top to bottom).

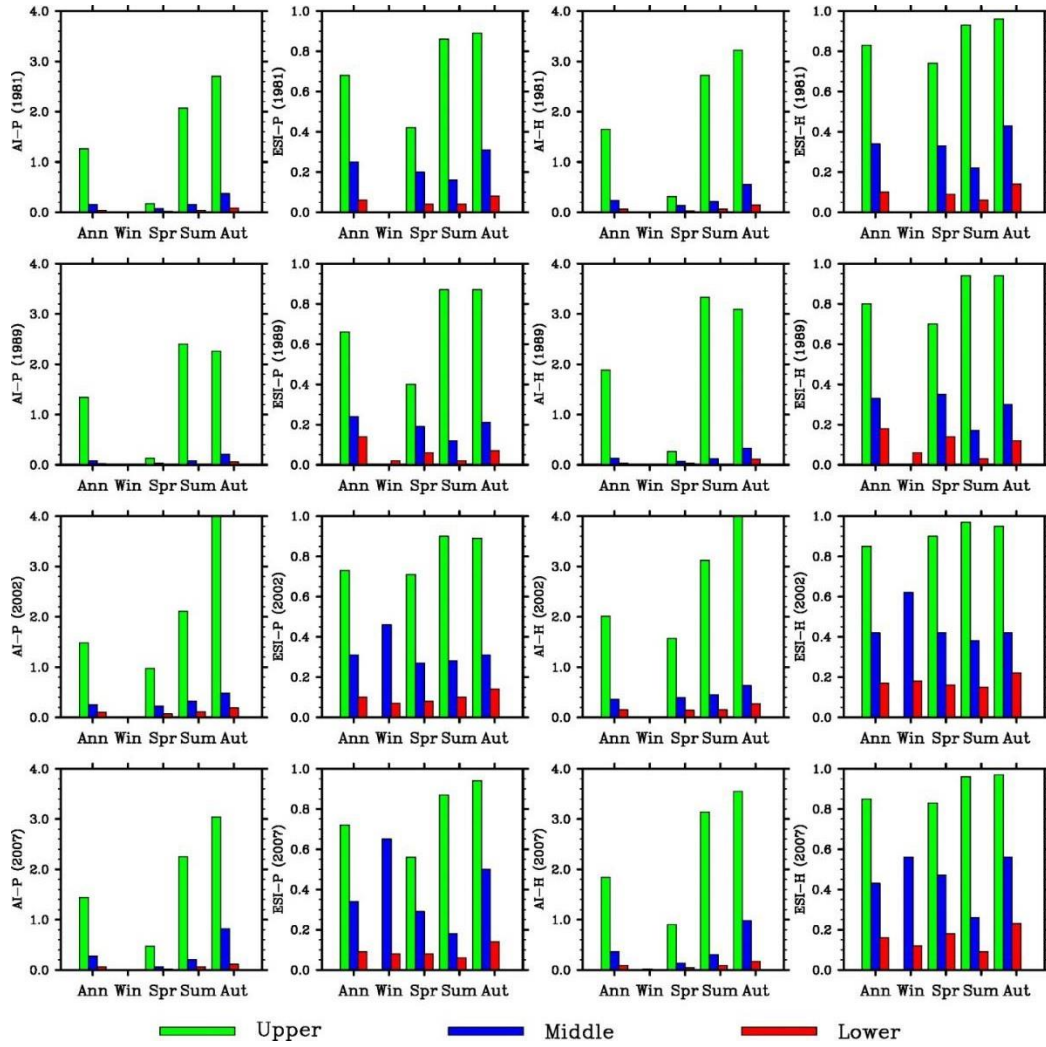


Figure 11. Seasonal variations of simulated Aridity Index (*AI*), and Evaporative Stress Index (*ESI*) using the Penman-Monteith and Hamon methods (left to right) for the wet years of 1981, 1989, 2002, and 2007 (from top to bottom).

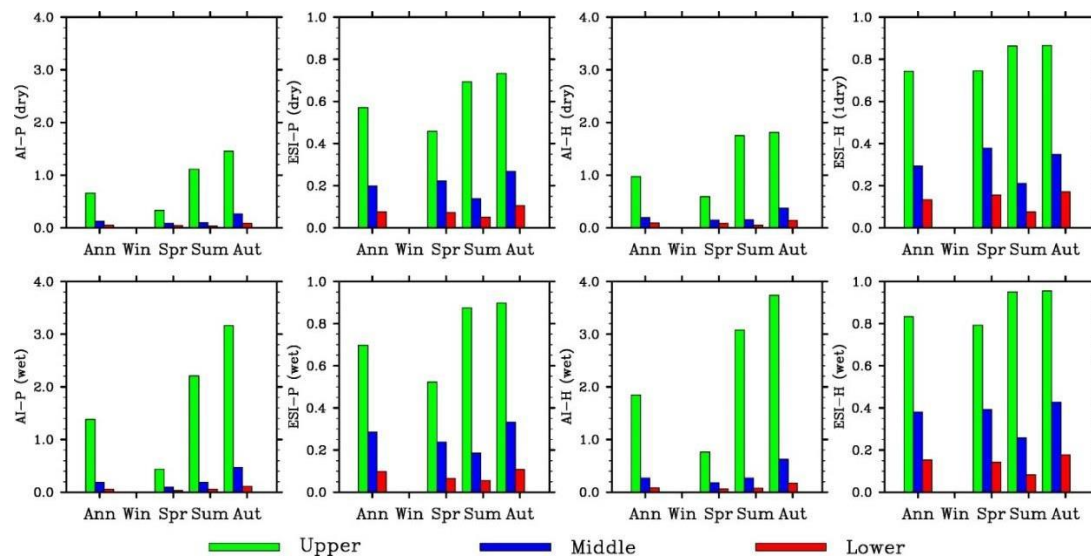


Figure 12. Seasonal variations of simulated Aridity Index (*AI*), and Evaporative Stress Index (*ESI*) using the Penman-Monteith and Hamon methods (left to right) for averages over the dry years of 1982, 1990, 2001, 2008 (top) and (bottom).

4 Discussion

4.1 Supports to the integrated water–ecosystem–economy study in the HRB

The HRB is a typical inland river basin with a strong contrast in topography, landscape, climate, and human activities from the headwater to end point along its drainage system.

Comprehensive monitoring, modeling, and data manipulation studies have been conducted for several decades to understand the hydrological and ecological processes and interactions in the HRB (Cheng et al., 2014). The middle HRB is a special region with dynamic land cover and use changes due to human activity. Different from the upper HRB regions where climate change has been the controlling factor for hydrological and ecological processes, surface water condition is extremely important in the middle HRB where irrigated farmland is the largest land use and natural oases have been gradually replaced by artificial oases (Li et al., 2001,

Cheng et al., 2014). According to our study, hydrological index ESI should be a better indicator than the meteorological index AI for water supply and demand conditions in the middle HRB.

Zhang et al. (2014) found that the streamflow from the upper to middle HRB has risen due to climate change, but the streamflow from middle to lower HRB has reduced. They attributed

this reduction to increasing water consumption by human activities in the middle HRB. Our

study indicates less dryness trend in the middle HRB and therefore supports the analysis that

climate change was not a major factor for the reduction. Sun et al. (2015) found an increasing

630 trend in vegetation growth in the middle HRB and attributed it to irrigation. Our study shows
631 less drying trend in this region, suggesting that more net water was another contributor to the
632 increasing vegetation growth.

634 **4.2 Importance of land-surface processes**

635
636 The water shortage and frequent droughts are the biggest environmental threat to the
637 ecosystems and human activities in the HRB as well as entire northwestern China. This
638 comparison study provides evidence for the importance of water and energy interactions
639 between land process and the atmosphere and between upstream and downstream in
640 determining climate types in an arid climate. Because the *ESI* values are related to *AET* that is
641 controlled by land-surface properties and management practices (e.g., rainfall-fed crops vs
642 irrigated crops; natural wetlands vs cultivated drained croplands), our results suggest the land-
643 surface processes play an important role in affecting aridity conditions. The landscape in the
644 HRB, especially its transition zone, has changed remarkably in the past several decades due to
645 urbanization, farming, and grazing activities (Hu et al., 2015). The irrigation may have caused
646 the lower basin more water stressed (higher *ESI* than *AI*) since stream water from Heihe is
647 intercepted and rivers go dry downstream. The *ESI* should reflect this change since it is
648 calculated partially based on the land-surface hydrological conditions. Urbanization, farming,
649 and grazing would reduce vegetation coverage. This would further reduce evapotranspiration
650 and increase runoff. Irrigation would play opposite roles. The RIEMS model uses the
651 Biosphere and Atmosphere Transfer Scheme (BATS) (Dickinson and Henderson-Sellers, 1993)
652 to simulate the land-surface hydrological processes. The vegetation and soil properties
653 measured in the HRB in 2000 were used to replace the universal BATS specifications, which
654 improved precipitation simulation (Xiong and Yan, 2013). However, the above disturbance
655 over time were not included in the simulation that provided the data for this study. Numerical
656 experiments with this model are needed to provide quantitative evidence for the hydrological
657 effects of the disturbances.

658 659 **4.3 Role in moderating climate**

660 The magnitude of *AI* (*ESI*) inter-annual variability in the middle basin is (is not) very close to
661 that in the lower basin, another evidence for the unique capacity of *ESI* in separating the climate
662 zones between the middle and lower basin reaches. The magnitude of the relative inter-annual
663 variability differs mainly between *AI* and *ESI*, larger with *AI*. In addition, both *AI* and *ESI* in
664 the HRB decreased dramatically from 1980 to 2010, at greater rate with *AI*. Thus, the aridity
665 conditions described using *ESI* is less variable, suggesting the role of local hydrological
666 processes in moderating extreme climate events.

667

668 **4.4 Future trends**

669

670 One of the hydrological consequences from the projected climate change due to the greenhouse
671 gas increase is more frequent and intense droughts in watersheds of dry regions. In the
672 Colorado River Basin, global warming may lead to substantial water supply shortages
673 (McCabe and Wolock, 2007), and the climate models projected considerably more drought
674 activities in the 21st century (Cayan et al., 2010). In the HRB, the climate of the upper HRB
675 will likely become warmer and wetter in the near future (Zhang et al., 2016), consistent with
676 the historical records. Correspondingly the basin-wide evapotranspiration, snowmelt, and
677 runoff are projected to increase over the same period. Many aridity indices, including the *AI*,
678 have been used to project future aridity trends (Paulo et al., 2012). However, most of the recent
679 *ESI* studies are based on historical remote sensing for monitoring short-term drought
680 development, which limits the application of this index to climate change impact research. Due
681 to the unique ability with the *ESI* in identifying the transition climate zone as shown in this
682 study, it would be valuable to explore its potential for future aridity projection study and
683 compare with that of the *AI*.

684

685 **4.5 Uncertainty and future research**

686

687 The regional climate simulation which generated data for this analysis has many uncertainties
688 (Xiong and Yan, 2013). One of the contributing factors is the very limited number of
689 meteorological, hydrological, and ecological measurement sites. A large-scale, multiple-year
690 field experiment project has been conducted in the HRB, which have been generating extensive
691 datasets (Wang et al., 2014). These data are being used to improve the regional climate

692 modeling, which will in turn generate new high-resolution data for further aridity analysis.
693 Furthermore, the regional climate modeling has been expanded into the middle 21st century,
694 providing data for calculating the aridity indices and comparing their future trends.
695 Comparisons of other meteorological and hydrological aridity indices are also a future research
696 issue.

697

698 **5 Conclusions**

699

700 This study has found that the *ESI* climate classification agrees with the Koppen climate
701 classification (Peel et al., 2007). By using *ESI*, we found that the climate types are different
702 among the upper, middle, and lower HRB. In contrast, there is no difference between the
703 middle and lower HRB regions when the *AI* is used. The comparison results from this study
704 therefore suggest that only *ESI* is able to identify a transition climate zone between the
705 relatively humid climate in the mountains and the arid climate in the Gobi desert region. We
706 conclude that the hydrological aridity index *ESI* is a better index than the meteorological aridity
707 index *AI* for climate classification in the HRB with a complex topography and land cover.
708 Selection of the most appropriate aridity index facilitates climate characterization and
709 assessment, risk mitigation, and water resources management in the arid region.

710

711 **Acknowledgement** This study was supported by the National Natural Science Foundation of
712 China (NSFC) (No. 91425301) and the USDA Forest Service. We thank the reviewers for
713 valuable and insightful comments and suggestions.

714

715 **References**

- 716 Allen, R. G., Pereira, L. S., Raes, D., and Smith, M.: “Crop evapotranspiration: guidelines for
717 computing crop water requirements.” Irrigation and Drainage Paper No. 56, Food and
718 Agriculture Organization of the United Nations, Rome, Italy, 1998.
- 719 Anderson, M. C., Hain, C. R., Wardlow, B., Mecikalski, J. R., and Kustas, W. P.: Evaluation
720 of drought indices based on thermal remote sensing of evapotranspiration over the
721 continental U.S. *Journal of Climate*, 24, 2025–2044, 2011.
- 722 Anderson, M. C., Zolin, C. A., Sentelhas, P. C., Hain, C. R., Semmens, K., Yilmaz, M. T., Gao,
723 F., Otkin, J. A., and Tetrault, R.: The Evaporative Stress Index as an indicator of agricultural

drought in Brazil: An assessment based on crop yield impacts, *Remote Sensing of Environment*, 174, 82–99, doi:10.1016/j.rse.2015.11.034, 2016.

Budyko, M. I.: *Climate and Life*, Academic, San Diego, CA, 508 pp., 1974.

Cayan, D. R., Das, T., Pierce, D. W., Barnett, T. P., Tyree, M., and Gershunov, A.: Future dryness in the southwest US and the hydrology of the early 21st century drought, *Proc. Natl. Acad. Sci.*, 107, 21, 271–21, 276. <http://research001.com/?showinfo-140-577279-0.html>, 2010.

Chen, Y., Zhang, D., Sun, Y., Liu, X., Wang, N., and Savenije, H.: Water demand management: A case study of the Heihe River Basin in China. *Phys. Chem. Earth*, 30, 408–419, <http://dx.doi.org/10.1016/j.pce.2005.06.019>, 2005.

Cheng, G.D., Li, X., Zhao, W.Z., Xu, Z.M., Feng, Q., Xiao, S.C., Xiao, H.L.: Integrated study of the water–ecosystem–economy in the Heihe River Basin, *National Science Review*, 1: 413–428, doi: 10.1093/nsr/nwu017, 2014.

Choi, M., Jacobs, J. M., Anderson, M. C., and Bosch, D. D.: Evaluation of drought indices via remotely sensed data with hydrological variables, *Journal of Hydrology*, 476, 265–273. doi:10.1016/j.jhydrol.2012.10.042, 2013.

Dickinson, R.E., Henderson-Sellers, A.: *Biosphere-Atmosphere Transfer Scheme (BATS) Version as coupled to the NCAR Community Climate Model*, NCAR Technical Report, NCAR/TN-387+STR, 1993.

Gao, B., Qin, Y., Wang, Y. H., Yang, D., and Zheng, Y.: Modeling Ecohydrological Processes and Spatial Patterns in the Upper Heihe Basin in China, *Forests*, 7(1). doi:10.3390/f7010010, 2016.

Guttman, N.B.: Accepting the standardized precipitation index: a calculation algorithm. *JAWRA Journal of the American Water Resources Association*, John Wiley & Sons, 35 (2): 311–322. doi:10.1111/j.1752-1688.1999.tb03592.x. 1999.

Hamon, W. R.: Computation of direct runoff amounts from storm rainfall. *Intl. Assoc. Scientific Hydrol. Publ.*, 63, 52–62, 1963.

Hu, X., Lu, L., Li, X., Wang, J., and Guo, M.: Land use/cover change in the middle reaches of the Heihe River Basin over 2000–2011 and its implications for sustainable water resource management. *PLoS ONE* 10(6): e0128960. doi:10.1371/journal.pone.0128960, 2015.

754 Huschke, R. E.: Glossary of Meteorology, American Meteorological Society, Boston, 1959. (Second
755 printing-1970).

756 Keetch, J.J., Byram, G.M.: A drought index for forest fire control. USDA Forest Service
757 Research Paper No. SE38, pp. 1–32.1968.

758 Li, J., Multivariate Frequencies and Spatial Analysis of Drought Events Based on
759 Archimedean Copulas Functio, Northwest University of Science and Technology, 2012.
760

761 Li, X., Lu, L, Cheng, G.D., Xiao, H.L.: Quantifying landscape structure of the Heihe River
762 Basin, north-west China using FRAGSTATS, Journal of Arid Environments, 48: 521–535,
763 doi:10.1006/jare.2000.0715, 2001.

764 Maliva, R., Missimer, T.: Arid Lands Water Evaluation and Management,
765 <https://www.springer.com/us/book/9783642291036>, P 21-39. 2012.

766 McCabe, G. J., and Wolock, D. M.: Warming may create substantial water supply shortages in
767 the Colorado River basin, Geophysical Research Letters, 34, 22, 2007.

768 McKee, T.B., Doesken, N.J., Kleist, J.: The Relationship of Drought Frequency and Duration
769 to Time Scales. Proceedings of the Eighth Conference on Applied Climatology. American
770 Meteorological Society: Boston; 179–184, 1993.

771 Nalbantis, I. and Tsakiris, G. Assessment of hydrological drought revisited Water Resour.
772 Manag. 23 881–97, 2009.

773 Narasimhan, B., and Srinivasan, R.: Development and evaluation of soil moisture deficit index
774 and evapotranspiration deficit index for agricultural drought monitoring. Agricultural and
775 Forest Meteorology, 133, 69-88. 2005.

776 Onder, D., Aydin M., Berberoglu, S., Onder, S., and Yano, T.: The use of aridity index to
777 assess implications of climatic change for land cover in Turkey. Turkish Journal of
778 Agriculture and Forestry, 33, 305-314, 2009.

779 Otkin, J. A., Anderson, M. C., Hain, C. R., Mladenova, I. E., Basara, J. B., and Svoboda, M.:
780 Examining rapid onset drought development using the thermal infrared based Evaporative
781 Stress Index, Journal of Hydrometeorology, 14, 1057–1074, 2013.

782 Palmer, W.C.: Meteorological drought. U.S. Research Paper No. 45. US Weather Bureau,
783 Washington, DC, <https://www.ncdc.noaa.gov/temp-and-precip/drought/docs/palmer.pdf>.
784 1965.

785 Paulo, A. A., Rosa, R. D., and Pereira, L. S.: Climate trends and behavior of drought indices

based on precipitation and evapotranspiration in Portugal, *Nat. Hazards Earth Syst. Sci.*, 12, 1481–1491, 2012.

Peel, M. C., Finlayson, B. L., and McMahon, T. A.: Updated world map of the Köppen–Geiger climate classification. *Hydrol. Earth Syst. Sci.*, 11, 1633–1644. doi:10.5194/hess-11-1633-2007, 2007.

Ponce, V. M., Pandey, R. P., and Ercan, S.: Characterization of drought across climatic spectrum. *Journal of Hydrologic Engineering*, ASCE 5, 222–2245, 2000.

Ren, Z., Lu, Y., and Yang, D.: Drought and flood disasters and rebuilding of precipitation sequence in Heihe River basin in the past 2000 years, *J. Arid Land Resour. Environ.*, 24, 91–95, 2010.

Shukla, S., and Wood, A.W.: Use of a standardized runoff index for characterizing hydrologic drought. *Geophys. Res. Lett.*, 35, L02405. doi:10.1029/2007GL03248. 2008.

Sun, W., Song, H., Yao, X., Ishidaira, H., Xu, Z.: Changes in remotely sensed vegetation growth trend in the Heihe basin of arid northwestern China. *PLoS ONE*, 10(8): e0135376. doi:10.1371/journal.pone.0135376, 2015.

Svoboda, M., LeComte, D., Hayes, M., Heim, R., Gleason, K., Angel, J., Rippey, B., Tinker, R., Palecki, M., Stooksbury, D., Miskus, D., and Stephin, S.: The Drought Monitor, *Bulletin of the American Meteorological Society*, 83, 1181–90, 2002.

UNESCO, Map of the World Distribution of Arid Regions. MAB Techn. Note 7, 1979.

Wolfe, S. A.: Impact of increased aridity on sand dune activity in the Canadian Prairies. *Journal of Arid Environments*, 36, 421–432, 1997.

Wang, L. X., Wang, S. G., and Ran, Y. H.: Data sharing and data set application of watershed allied telemetry experimental research, *IEEE Geoscience and Remote Sensing Letters*, 11, 2020–2024, 10.1109/LGRS.2014.2319301, 2014.

Wilhite, D. A. and Glantz, M. H.: Understanding the drought phenomenon: The role of definitions. *Water International* 10:111–20. 1985.

Woodhouse, C. A., Meko, D. M., MacDonald, G. M., Stahle, D. W., and Cook, E. R.: A 1,200-year perspective of 21st century drought in southwestern North America. *Proc. Natl. Acad. Sci. USA*, 107, 21283–21288, 2010.

Xiong, Z., and Yan, X. D.: Building a high-resolution regional climate model for the Heihe River Basin and simulating precipitation over this region. *Chin. Sci. Bull.*, 58, 4670–4678,

817 Yang, D. W., Gao, B., Jiao, Y., Lei, H. M., Zhang, Y. L., Yang, H. B., and Cong, Z. T.: A
 818 distributed scheme developed for eco-hydrological modeling in the upper Heihe River. *Sci.*
 819 *China Earth Sci.*, 58, 36–45. <http://dx.doi.org/10.1007/s11430-014-5029-7>, 2015.
 820 Yang, G. H.: *Agricultural Resources and Classification*, China Agricultural Press, Beijing,
 821 China, 286 pp., 2007.
 822 Yao, A. Y. M.: Agricultural potential estimated from the ratio of actual to potential
 823 evapotranspiration, *Agricultural Meteorology*, 13, 405-417, doi:
 824 10.1016/0002-1571(74)90081-8, 1974.
 825 Zhang, A. J., Liu, W. B., Yin, Z. L., Fu, G. B., and Zheng, C. M.: How will climate change affect the
 826 water availability in the Heihe River Basin, Northwest China? *J.*
 827 *Hydrometeorology*, doi: <http://dx.doi.org/10.1175/JHM-D-15-0058.1>, 2016.
 828 Zargar, A., Sadiq, R., Naser, B., and Khan, F. I.: A review of drought indices. *Environmental*
 829 *Reviews*, 19, 333–349. 2011.
 830 Zhang, A.J., Zheng, C.M., Wang, S., Yao, Y.Y.: Analysis of streamflow variations in the
 831 Heihe River Basin, northwest China: Trends, abrupt changes, driving factors and ecological
 832 influences, *Journal of Hydrology: Regional Studies* 3, 106–124, 2015.
 833